Earthq Eng & Eng Vib (2017) 16: 349-364 **DOI**: 10.1007/s11803-017-0386-9

Research on seismic behavior and shear strength of SRHC frame columns

Zheng Shansuo[1†], Qin Qing[1,2‡], Zhang Yixin[1†], Zhang Liang[1†] and Yang Wei[1†]

1. *Department of Civil Engineering, Xi'an University of Architecture and Technology, Xi'an 710055, China*
2. *Department of Civil and Architecture Engineering, Xi'an University of Science and Technology, Xi'an 710054, China*

Abstract: The seismic behavior of steel reinforced high strength and high performance concrete (SRHC) frame columns was investigated through pseudo-static experiments of 16 frame columns with various shear span ratios, axial compression ratios, concrete strengths, steel ratios and stirrup ratios. Three kinds of failure mechanisms are presented and the characteristics of experimental hysteretic curves and skeleton curves with different design parameters are discussed. The columns' ductility and energy dissipation were quantitatively evaluated based on seismic resistance. The research results indicate that SRHC frame columns can withstand extreme bearing capacity, but the abilities of ductility and energy dissipation are inferior because of SRHC's natural brittleness. As a result, the axial load ratio should be restricted and some construction measures adopted, such as increasing the stirrup ratio. This research established effect factors on the bearing capacity of SPHC columns. Finally, an algorithm for obtaining ultimate bearing capacity using the flexural failure mode is established based on a modified plane-section assumption. The authors also established equations to determine shearing baroclinic failure and shear bond failure based on the accumulation of the axial load force distribution ratio. The calculated results of shear bearing capacity for different failure modes were in good agreement with the experimental results.

Keywords: SRHC frame columns; seismic behavior; ductility; energy dissipation; axial compression ratio; shear bearing capacity

1 Introduction

Earthquake investigations and experimental studies have verified that the seismic behavior of steel reinforced concrete (SRC) structures is obviously better than that of reinforced concrete (RC) structures (Ji *et al*., 2015). For lower stories in high-rise buildings, the carrying capacity of a SRC frame column cannot satisfy the seismic demand due to the poor ductility arising from the small shear span ratio. Nevertheless, the SRHC frame column possesses significant advantages. As an optimized combination of high-tech concrete material and new-style composite structures, steel reinforced high strength and high performance concrete (SRHC) structures possesses excellent mechanical performance and seismic behavior, and are being used more often in engineered structures. Zheng *et al*. (2011) discussed the damage evolution in steel reinforced high strength concrete (SRHSC) frame columns based on the test results of cyclic reversed loading experiments on 12 frame column specimens, which resulted in a damage model that can well reflect the mechanical characteristics of SRHSC members subjected to horizontal earthquake action. Yan *et al*. (2010) investigated the seismic performance of a composite frame comprised of steel reinforced ultra high-strength concrete (SRUHSC) columns and steel reinforced concrete (SRC) beams. Lu *et al*. (2015) presented an experimental study on the compressive behavior of steel fiber reinforced high strength concrete-filled steel tube columns. A new deck system for moveable bridges was developed that makes use of ultra-high performance concrete (UHPC) reinforced with high strength steel (HSS) rebars to achieve light weight and high strength requirements. Xia *et al*. (2011) investigated the mechanism of the deck strip shear failure experimentally and analytically. Kamal *et al*. (2014) aimed to evaluate the behavior of ultra-high strength concrete beams; a total of 12 simple concrete beams with and without shear reinforcements were tested in flexure. Despite ongoing worldwide efforts to improve concrete, more thorough and systematic experimental research is needed on the seismic behavior of SRHC frame columns. This is especially true when the concrete strength grade exceeds C100 (Li *et al*.,

Correspondence to: Qin Qing, Department of Civil Engineering, Xi′an University of Architecture and Technology, Xi′an 710055, China
Tel: +86-13572229454
E-mail: qinqingjd@163.com
[†]Professor; [‡]PhD

Supported by: National Key Technology R&D Program under Grant No. 2013BAJ08B00 and the Natural Science Foundation of China under Grant Nos. 50978218 and 51108376
Received January 27, 2016; **Accepted** July 25, 2016

2007a; Abed *et al*., 2013).

Therefore, the column element between the points of inflection of the frame structure was selected as a focal point, and the seismic behavior of 16 SRHC frame column specimens were studied from every aspect including their mechanical characteristics, failure mode, bearing capacity, hysteretic behavior, ductility and energy dissipation. Furthermore, limited values of the axial load ratio and minimum stirrup ratio are proposed based on ductility tests and results. Finally, research on SRHC columns' shear bearing capacity for different failure modes is presented through systematic testing and calculations. The experimental results and theoretical derivation provide a basis for establishing a novel and potentially transformation design theory for SRHC frame columns.

2 Experiment program

2.1 Test specimen

There are several main parameters that have great influence on the seismic behavior of SRHC frame columns, such as shear span ratio, axial compression ratio, concrete strength, stirrup ratio, steel ratio, concrete covering layer thickness and loading mode (Wang, 2005). Therefore, different levels of these parameters are taken into consideration in the experiment, including shear span ratio, 1.32–3.27; axial compression ratio, 0.21–0.36; concrete strength, 69.75–117.42 MPa; stirrup ratio, 1.26%–1.72%, and steel ratio 4.7% and 5.6%. Sixteen SRHC frame columns containing solid-web steel were designed based on Chinese code JGJ138-2001 (2001). The cross section size of the columns was 160 mm × 240 mm. Table 2 lists the parameters of the ordinary I14 and I12.6 hot-rolled I-beam steel used in the experiments. Longitudinal reinforcements for concrete were Grade HRB335, and the stirrups were Grade HPB235. The values of the primary study variables are summarized in Table 1. Table 2 shows the properties of the reinforcement bars and steel. Figure 1 shows the plan views and important reinforcement and steel details for the specimens.

2.2 Test set-up

The experiment adopts a cantilever beam quasi-static loading system and was conducted in the Structure and Seismic Laboratory of Xi'an University of Architecture and Technology. First, the target vertical load was exerted on the specimens via hydraulic jacks. Then, the actuator attached to the top of the specimen through the lateral load transfer assembly applied the lateral load; the vertical load was held constant throughout the testing process. Prior to the yielding of the specimen, the lateral load mode was exerted by the force-controlled load transfer assembly. After the specimen yielded, 2–3 cycles of loading and unloading were conducted for each subsequent displacement level, which was increased by multiples of the yield displacement. When the bearing capacity of the columns dropped to 70 percent of the peak load, loading ended. The test data were collected by a 1000-channel data acquisition instrument, and the entire testing process was controlled automatically by servo controllers and a computer. The loading sketch and system are shown in Fig. 2. Figure 3 illustrates the loading history of beam-column subassemblies.

Table 1 Design parameters of specimens

Item	f_{cu} (MPa)	L_c (mm)	λ	n_t	s (mm)	ρ_v (%)	ρ_s (%)
SRHC-5	79.6	870	3.27	0.28	ϕ 6 @ 60	1.38	5.60
SRHC-6	85.5	750	2.73	0.31	ϕ 6 @ 60	1.38	5.60
SRHC-7	79.4	630	2.18	0.28	ϕ 6 @ 60	1.38	5.60
SRHC-8	108.6	510	1.64	0.32	ϕ 6 @ 60	1.38	5.60
SRHC-9	78.5	440	1.32	0.22	ϕ 6 @ 60	1.38	5.60
SRHC-10	80.2	510	1.64	0.22	ϕ 6 @ 60	1.38	5.60
SRHC-11	79.4	510	1.64	0.36	ϕ 6 @ 60	1.38	5.60
SRHC-12	96.1	510	1.64	0.26	ϕ 6 @ 60	1.38	5.60
SRHC-13	117.4	510	1.64	0.31	ϕ 6 @ 60	1.38	5.60
SRHC-14	81.1	510	1.64	0.28	ϕ 6 @ 60	1.38	5.60
SRHC-15	69.8	870	3.27	0.26	ϕ 6 @ 60	1.38	5.60
SRHC-16	107.1	870	3.27	0.27	ϕ 6 @ 60	1.38	5.60
SRHC-17	115.5	870	3.27	0.31	ϕ 6 @ 60	1.38	5.60
SRHC-18	77.7	630	2.18	0.24	ϕ 8 @ 120	1.26	5.60
SRHC-19	80.7	630	2.18	0.23	ϕ 8 @ 90	1.72	5.60
SRHC-20	75.7	630	2.18	0.21	ϕ 8 @ 120	1.26	4.70

Notes: f_{cu} is the prismatic compressive strength of concrete; L_c is the total length of the top and bottom column; λ is the shear span ratio; n_t is the axial force; s is the stirrup spacing; ρ_v is the volume-stirrup ratio; ρ_s is the steel ratio

Table 2 Mechanical properties of reinforcement bars and steel

Model of steel	f_y (MPa)	f_u (MPa)	E_s (MPa)
Flange girth of I14/I12.6 steel	319.7	426.5	2.07×10^5
Web plate of I14/ I12.6 steel	312.4	417.2	2.07×10^5
ϕ10 reinforced bar	386.3	495.7	2.06×10^5
ϕ6 hoop reinforcement	397.5	528.6	2.07×10^5
ϕ8 hoop reinforcement	354.1	447.3	2.07×10^5

Notes: f_y is the yielding strength; f_u is the ultimate strength; E_s is the elastic modulus

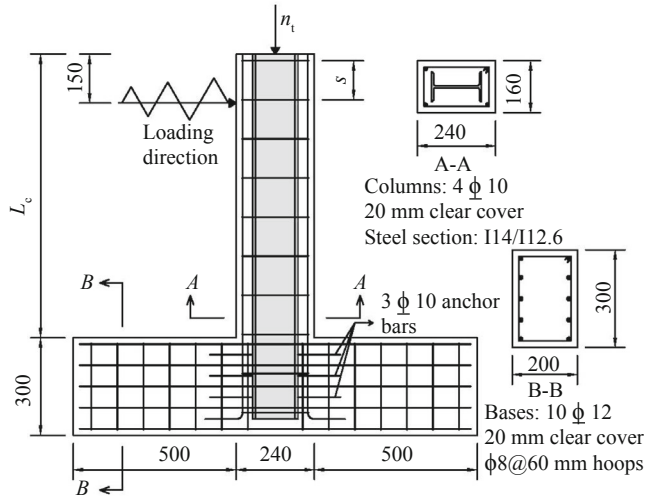

Fig. 1 Size and arrangement of reinforcement and steel components

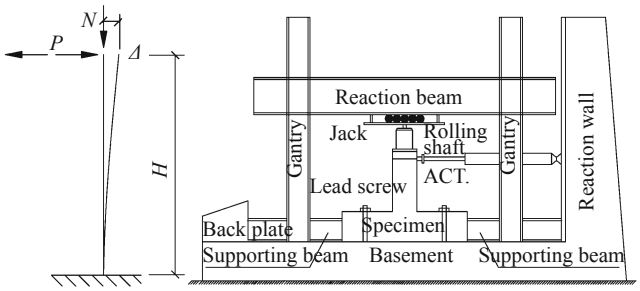

Fig. 2 Test setup and arrangement of instruments

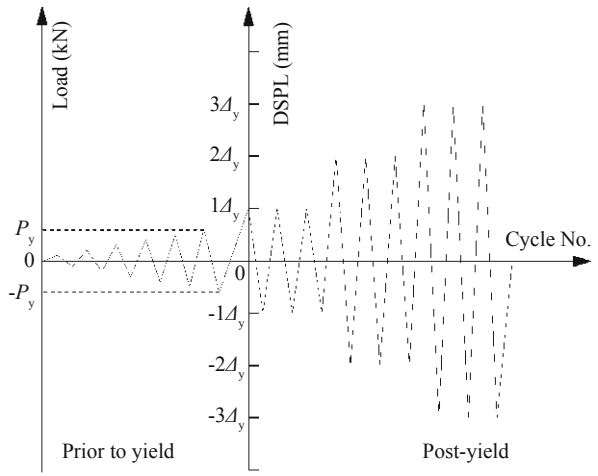

Fig. 3 Loading protoco

2.3 Test content

Measurement configurations with exterior apparatus are shown in Fig. 4. Linear variable displacement transducers (LVDTs) and an inclinometer were installed to monitor the lateral displacement and the angles of the central axis. The axial force and horizontal load at the top of the pillar are documented by a pull-pressure sensor. Furthermore, in order to measure the flexural and shearing deformation at the base of the pillar, a number of deformeters were set up. Finally, strains of longitudinal reinforcement bars, stirrups and steel were measured by strain gauges as shown in Fig. 5.

3 Experimental results

3.1 Failure mode

According to the experimental results, the failure modes of the SRHC columns can be divided into flexural failure mode, shearing bond failure mode and shearing baroclinic failure mode. These three failure modes are shown in Figs. 6–8, respectively.

When the shear span ratio of the SRHC columns is small ($\lambda \leq 1.64$), diagonal cracks appear near the central axis in the mid sections of the specimen until the horizontal load reaches 57%–75% P_{max}. A few vertical cracks synchronously appeared on the outside of the compressed steel flange. When the horizontal load reached between 84% and 91%P_{max}, "X" cracks with an approximate 45° diagonal line emerged, which divided the shearing-compression sector of the column into some prisms. Finally, because of the baroclinic prisms were crushed, the SRHC columns could no longer be used due to the shearing baroclinic failure mode as shown in Fig. 6.

When the shear span ratio is moderate ($1.64 < \lambda < 2.73$), vertical bond cracks will suddenly appear on the outside of the compressed steel flange and develop rapidly until the horizontal load reaches 61%–67% P_{max}, and the cracks are uniformly distributed along the column; then, the adhesion stress between steel and concrete will

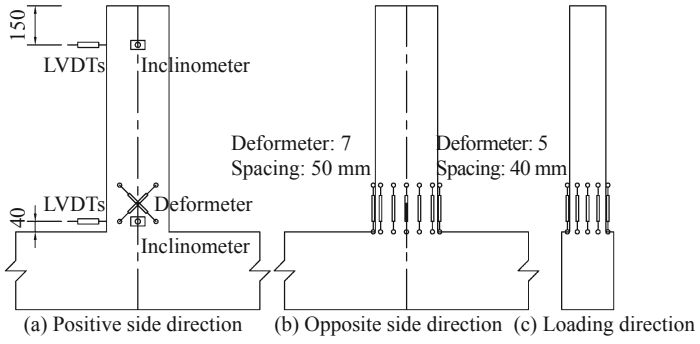

Fig. 4 Exterior apparatus

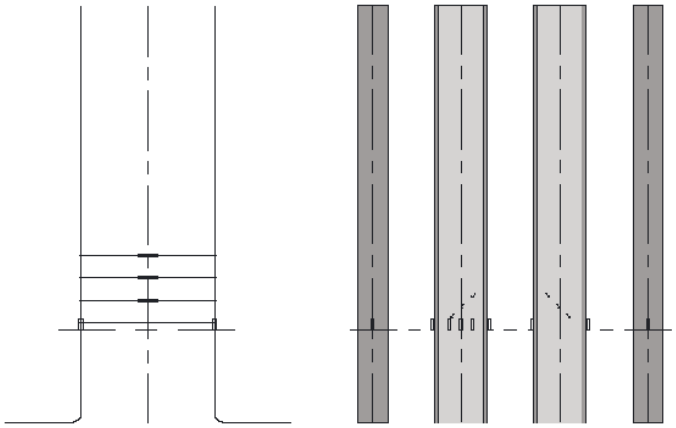

(a) Reinforcement cage (b) Flange and web of I steel

Fig. 5 Arrangement of interior strain gauges

initiate the process of gradual degeneration. Finally, the main longitudinal bond-splitting crack is formed, and the SRHC columns are further damaged in the shearing bond failure mode as shown in Fig. 7.

When the shear span ratio is comparatively large ($\lambda \geq 2.73$), the horizontal flexural cracks first appear at the bottom of the specimens until the horizontal load reaches 58%–75% P_{max}. When the compressive zone of the concrete reaches the ultimate compression strain, the reinforced steel bars gradually yield. The bottom corner is finally crushed thereby destroying any functional use of the SRHC columns according to the flexural failure mode as shown in Fig. 8. The characteristic values of specimens with their four damage states and failure modes are listed in Table 3.

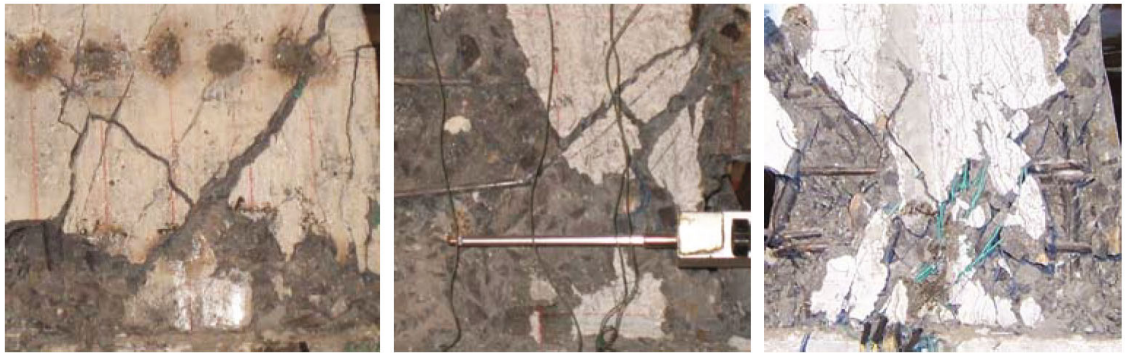

(a) SRHC-10 (b) SRHC-11 (c) SRHC-12

Fig. 6 Shearing baroclinic failure

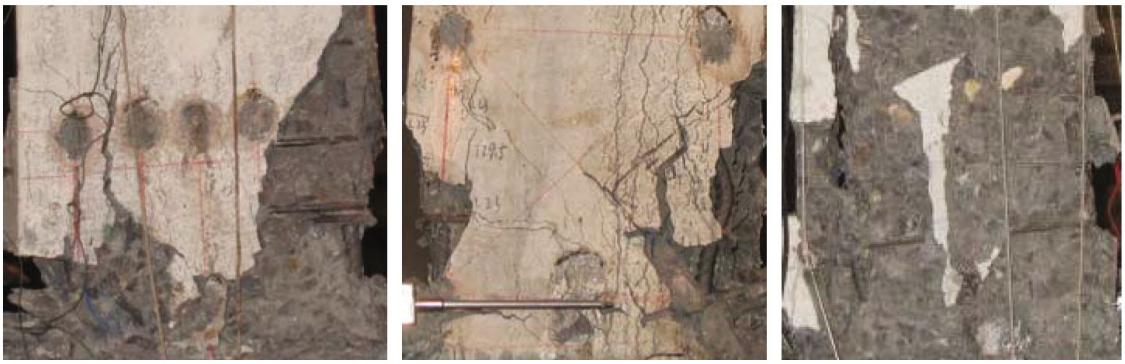

(a) SRHC-7 (b) SRHC-19 (c) SRHC-20

Fig. 7 Shearing bond failure

(a) SRHC-5 (b) SRHC-6 (c) SRHC-16

Fig. 8 Flexural failure

3.2 Hysteretic behavior

A load-deformation hysteretic curve is derived from a low cyclic reversed loading test of a structure, which includes a skeleton curve and hysteretic loop. Hysteretic behavior is an important basis for assessing the seismic performance of structures because it can be used to systematically analyze and predict the performance of several properties including stiffness and strength degradation, energy dissipation capacity, and ductility. The cycles of measured load-displacement hysteretic curves of SRHC frame columns are shown in Fig. 9. When the horizontal load is less than the cracking load P_{cr}, the specimen is in the elastic stage, where the load-displacement (P-Δ) curves usually start out as a straight line. As the horizontal load increases, P-Δ curves gradually form a curve. The deformation rises quickly. After unloading, residual deformation appears as evidence of the specimen's elasto-plastic property. After reaching the point of yield, two cycles of loading and unloading are conducted for each subsequent displacement level. Loading stiffness greatly decreases as displacement increases. At the same displacement level, the slope and maximum bearing capacity are less than those of any given previous cycle. The stiffness and strength degradation becomes more pronounced as the cycles increase. After reaching the maximum horizontal load, the initial unloading curves become steep and the residual deformation is large enough to make the phenomenon of "displacement hysteresis" very evident. The characteristics of the hysteretic curves are described below along with the process involved as the different design parameters change.

(1) With an increasing shear span ratio, the maximum horizontal load begins to gradually decrease. After reaching the maximum horizontal load, the strength deterioration is slower and the hysteretic loops become thicker. Furthermore, in the case of inconspicuous strength reduction, the cycle index and ultimate displacement increase.

(2) As concrete strength increases, the maximum horizontal load gradually rises. Hysteretic loops become progressively thinner. After the maximum horizontal load, the limit deformation and stability of the hysteretic curve significantly decrease. Unfortunately, the bearing capacity deterioration accelerates.

(3) With an increase of the load ratio, the maximum bearing capacity will gradually increase; meanwhile, the stability of the hysteretic loops weakens after reaching their high peak point. This means that the columns experience less cycle numbers after the peak point. Hence, strength degradation significantly increases, and deformation is reduced.

(4) As stirrup and steel ratios increase, the maximum horizontal load also gradually increases, and hysteretic curves become thicker. The descending load branch becomes gentler, and the limit deformation heightens. Furthermore, the cycle index increases as the specimens' energy dissipation capacity intensifies.

Compared with reinforced high strength concrete (RHSC) columns (Bayrak and Sheikh, 1997), hysteretic behavior of the SRHC frame columns is in the ascendant. After the maximum horizontal load, there is no rapid overturn phenomenon. The hysteretic loops of the tested specimens were able to reach and maintain a stable state without obvious necking phenomenon primarily due to the excellent hysteretic behavior of the steel reinforcement.

Table 3 Characteristic values of specimens and their failure modes

Item	Crack		Yield		Ultimate		Failure		Failure mode
	P_{cr} (kN)	Δ_{cr} (mm)	P_y (kN)	Δ_y (mm)	P_{max} (kN)	Δ_{max} (mm)	P_u (kN)	Δ_u (mm)	
SRHC-5	121.69	2.79	131.56	4.53	161.34	7.01	137.14	16.72	Flexural
SRHC-6	137.22	2.37	190.50	4.27	226.77	8.95	192.75	15.36	Flexural
SRHC-7	164.58	3.98	238.43	5.36	270.27	8.08	229.73	17.90	Shearing bond
SRHC-8	217.10	1.95	314.37	3.52	359.63	5.23	305.69	9.52	Shearing baroclinic
SRHC-9	240.89	2.86	279.17	3.69	322.17	4.69	273.84	10.35	Shearing baroclinic
SRHC-10	187.37	2.30	262.53	4.08	312.74	7.05	265.83	13.85	Shearing baroclinic
SRHC-11	262.13	3.06	310.03	4.15	354.49	6.28	301.32	9.43	Shearing baroclinic
SRHC-12	210.71	2.06	288.11	3.56	366.30	5.27	311.36	16.58	Shearing baroclinic
SRHC-13	247.81	2.03	395.51	3.12	434.31	4.39	369.16	9.62	Shearing baroclinic
SRHC-14	231.18	1.73	308.22	3.79	339.23	5.97	288.35	9.73	Shearing baroclinic
SRHC-15	92.46	3.12	136.17	8.02	159.37	11.98	135.46	27.29	Flexural
SRHC-16	121.56	2.41	169.24	5.15	205.48	9.52	174.66	21.02	Flexural
SRHC-17	161.09	3.74	179.23	4.52	230.06	6.69	195.55	9.13	Flexural
SRHC-18	167.85	3.55	201.54	6.92	252.57	15.31	214.68	21.98	Shearing bond
SRHC-19	181.25	4.28	217.69	8.12	269.72	16.48	229.26	24.44	Shearing bond
SRHC-20	132.95	3.75	170.57	6.45	212.01	15.56	180.21	26.73	Shearing bond

Note: P_{cr}, P_y, P_{max} and P_u are the bearing capacities at crack, yield, ultimate and failure state respectively; Δ_{cr}, Δ_y, Δ_{max} and Δ_u are the corresponding lateral deflection

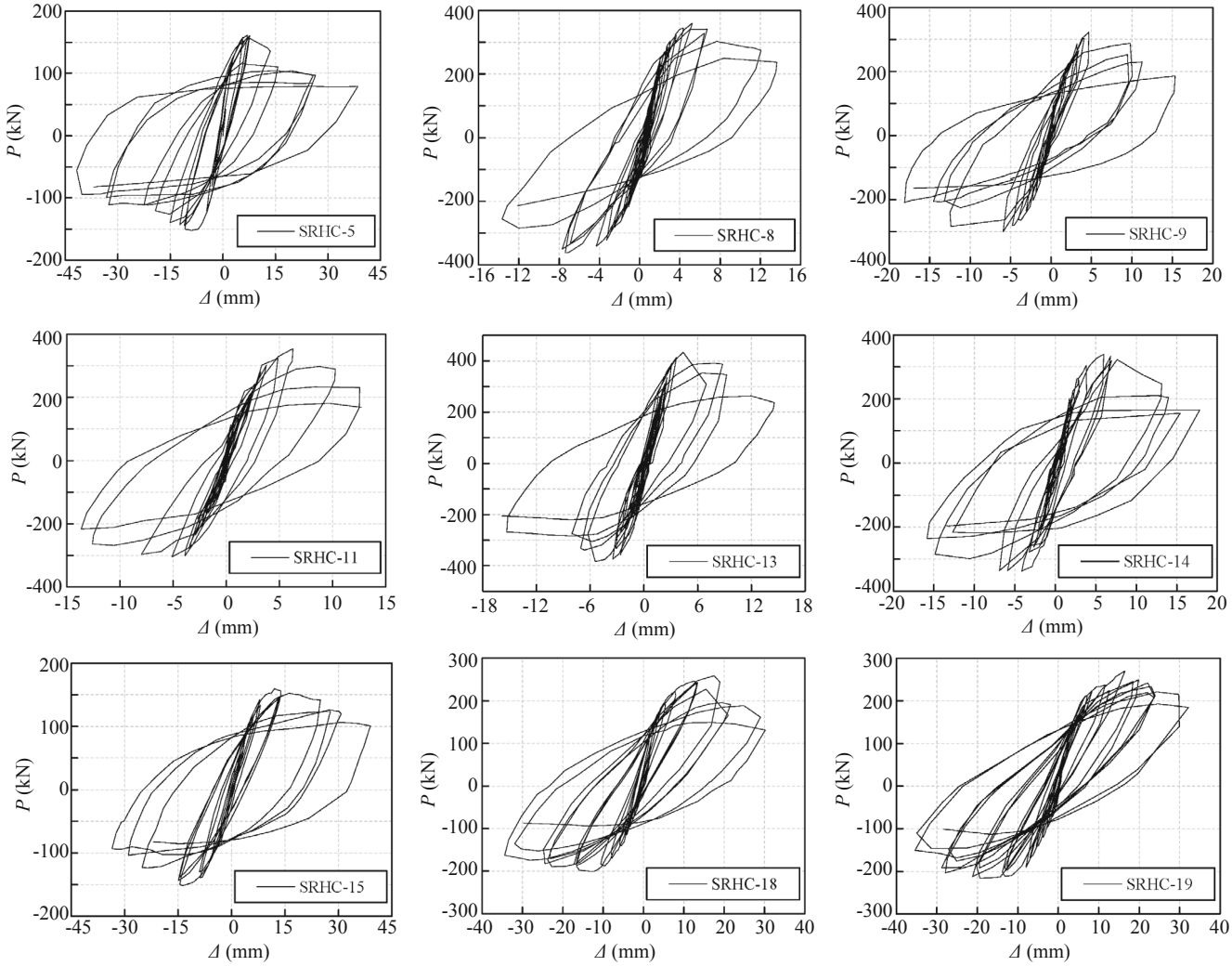

Fig. 9 *P-Δ* hysteretic curves

3.3 Skeleton curves

Skeleton curves of specimens are shown in Fig. 10. The loading process of the specimens can be roughly divided into four stages. 1) The elastic stage, when the horizontal load is less than approximately 50%–60% P_{max}, and the skeleton curves tend to form a line. 2) The elastic-plastic stage forms after concrete cracking; as the horizontal load increases, the curves gradually deviate from the straight line. 3) They then go through the steel yielding stage where the horizontal load is increased to approximately 80%–90% P_{max}; hence, the deformation grows rapidly. This leads to the failure stage. 4) After the peak point, the columns are destroyed because the bearing capacity drops so rapidly. The characteristics of the skeleton curves are described below according to their responses to property changes in the different stages.

(1) As the shear span ratio increases, the failure modes of the columns are shearing compression, shearing splitting and flexural failure in sequence. The ultimate bearing capacity decreased gradually, but meanwhile the ultimate displacement increases, and the descending branch of the curves tended to be smooth as shown in Fig. 10(a).

(2) As the concrete strength increases, the ultimate bearing capacity increased pronouncedly; however, the ultimate displacement gradually lessened. Meanwhile, the descending branch of the curves become steeper and steeper, and the ductility of the columns with high strength concrete is poor as shown in Figs. 10(c) and 10(d).

(3) As the load ratio increases, the initial stiffness of the columns increases, and the bearing capacity also increases slightly. However, the ultimate displacement gradually lessened. Due to the effect of *P-Δ*, the descending branch is so steep that the ductility of the columns with high load ratio is poor as shown in Fig. 10(b).

(4) As the stirrup and steel ratios increases, the ultimate bearing capacity and ultimate displacement increase significantly, and the descending branch tends to be gentle as shown in Figs. 10(e) and 10(f). The steel flanges and the stirrups provide an effective constraint

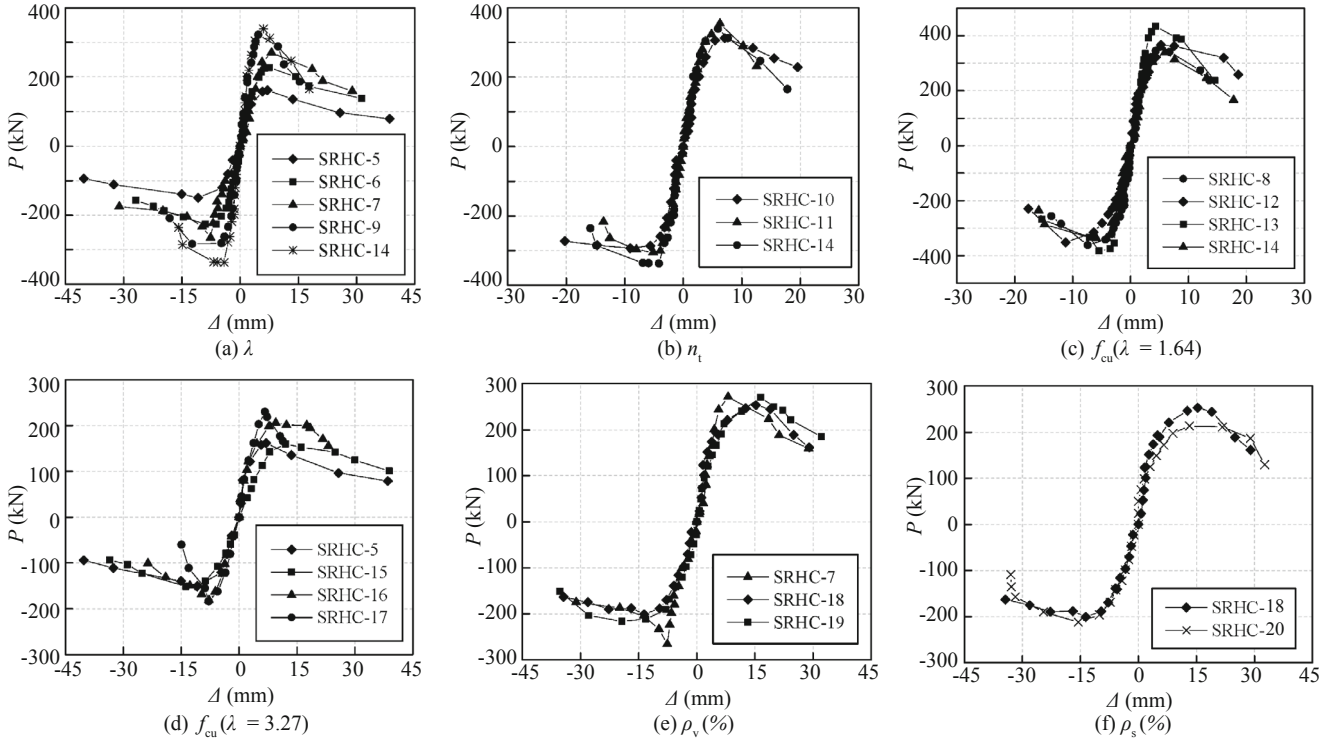

(a) λ (b) n_t (c) $f_{cu}(\lambda = 1.64)$

(d) $f_{cu}(\lambda = 3.27)$ (e) $\rho_v(\%)$ (f) $\rho_s(\%)$

Fig. 10 Skeleton curves

for the concrete. Therefore, the ductility of the columns with high stirrup ratios and steel ratios is better.

Compared with RC frame columns (Bae and Bayrak, 2008), the ductility and deformation capacity of SRHC frame columns are better. Moreover, the descending branch of the skeleton curves is gentler, and the bearing capacity deteriorates more slowly. However, compared with ordinary SRC frame columns (Ricles *et al*., 1994), because of the high strength and natural brittleness of high strength and high performance concrete (HSHPC), the bearing capacity of the SRHC frame columns measurably increases, and the descending branch of the skeleton curves is relatively steep. Plastic deformation capacity is also reduced.

3.4 Energy dissipation and ductility

The energy dissipation capacity can reflect nonlinear mechanical properties, which are an important index for measuring structural seismic performance. Generally, the energy dissipation capacity is measured by an equivalent viscous damping coefficient h_e and energy dissipation coefficient E (Clough and Penzien, 2003). The relationship between the equivalent viscous damping coefficient and horizontal displacement is shown in Fig. 11, and the energy dissipation indexes of the ultimate failure state are listed in Table 4.

The equivalent viscous damping coefficient of specimens increases as the horizontal displacement increases. Furthermore, the equivalent viscous damping coefficient in different cycles will change suddenly under same level of displacement. In a later stage of loading, the viscous damping coefficient can maintain a certain growth at a slow rate. These mean that the steel and its constrained inner concrete are still in good working condition and can continuously dissipate seismic energy, although the plastic deformation is increasing due to the concrete cover continuously crushing in the later stage of loading. As a result, SRCH columns have good post-seismic energy dissipation ability, which is more beneficial for resisting the second wave of seismic vibrations after a major earthquake.

As the shear span ratio increases, the equivalent viscous damping and energy dissipation coefficient of the specimens swell gradually, which indicates that the larger shear span ratio improves the seismic performance of the specimens, as shown in Fig. 11(a). As the concrete strength increases, the indexes of seismic energy dissipation capacity are reduced, as shown in Figs. 11(c) and 11(d); As the axial load ratio increases, the indexes reduce as shown in Fig. 11(b), which means that the ability to resist earthquakes decreases. As the stirrup ratio and steel ratio increase, the intensive ability of restraint for core concrete improves the plastic deformation capacity of the SHRC columns. Therefore, indexes of energy dissipation increase as the stirrup ratio increases and steel ratio increases, as shown in Figs. 11(e) and 11(f).

The displacement ductility factor are defined as $\mu_\Delta = \Delta u/\Delta y$, where Δu and Δy is the ultimate displacement and yield displacement, respectively. Δy and Δu can be defined by the energy equivalent method as shown in Fig. 12 (area $A_1 = A_2$, $P_u = 0.85P_{max}$). The specimen ductility factors are shown in Table 4. The relationship

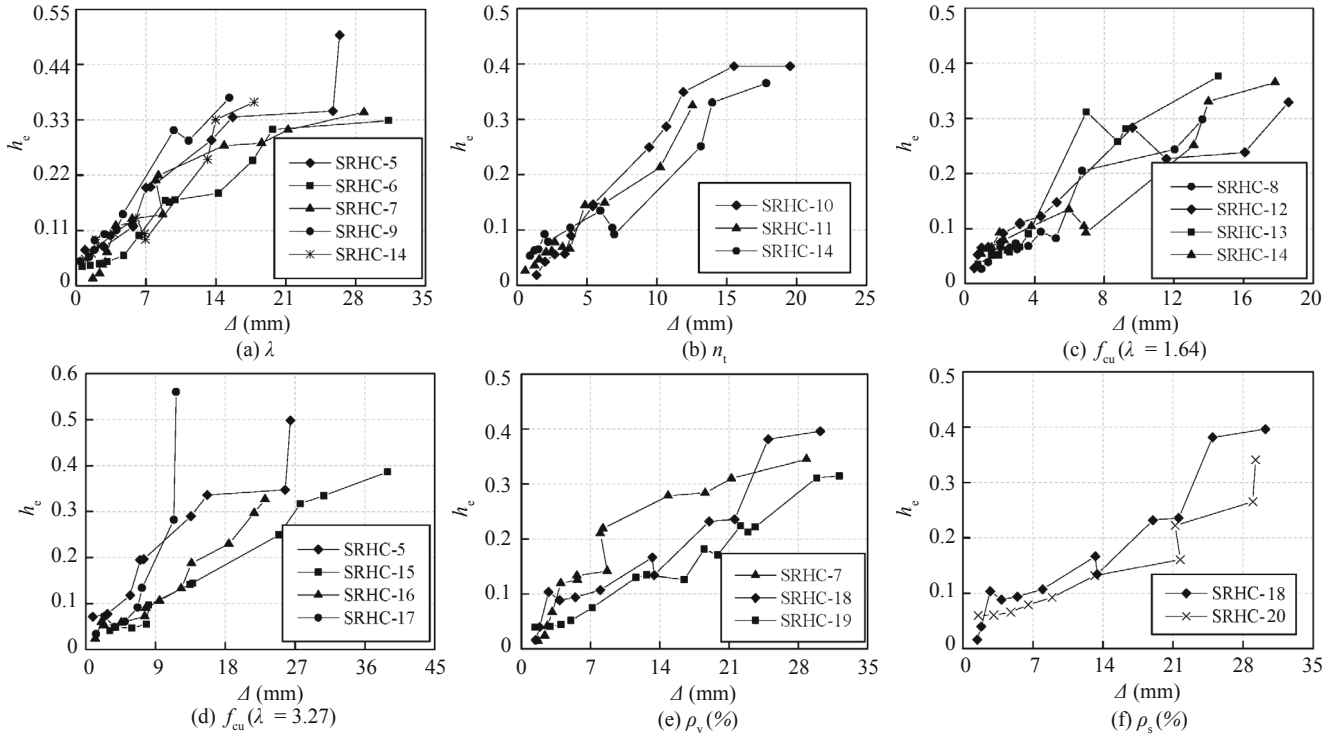

Fig. 11 The relationship between equivalent viscous damping coefficient and horizontal displacement

Table 4 Energy dissipation indexes of ultimate failure state and ductility factors

Item	h_e	E	μ_Δ	Item	h_e	E	μ_Δ
SRHC-5	0.32	1.73	3.62	SRHC-13	0.25	1.68	2.51
SRHC-6	0.25	1.35	3.59	SRHC-14	0.21	1.42	3.05
SRHC-7	0.26	1.61	3.12	SRHC-15	0.29	1.84	3.29
SRHC-8	0.22	1.22	2.71	SRHC-16	0.25	1.65	3.12
SRHC-9	0.31	1.69	2.92	SRHC-17	0.21	1.48	1.84
SRHC-10	0.37	1.59	3.14	SRHC-18	0.27	1.56	3.11
SRHC-11	0.18	1.27	2.77	SRHC-19	0.28	1.81	3.19
SRHC-12	0.27	1.39	2.86	SRHC-20	0.25	1.54	3.08

Notes: h_e is the equivalent viscous damping coefficient; E is energy dissipation factor; μ_Δ is displacement ductility factor.

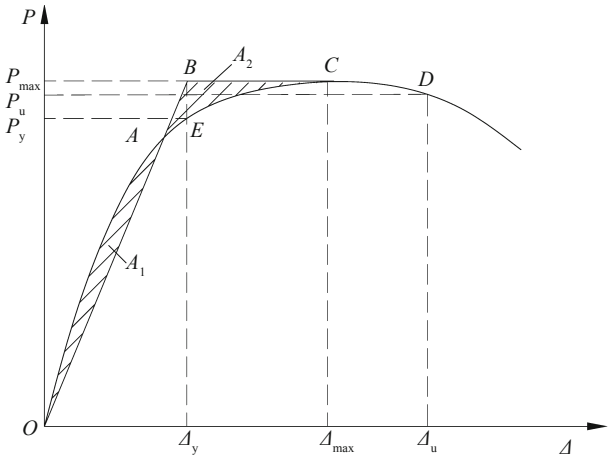

Fig. 12 Definition of yield and failure points

between the ductility factors and design parameters is illustrated in Fig. 13.

As the shear span ratio increases, the specimen ductility factor also increases. The shear span ratio mainly determines the failure modes based on the ductility of the specimens. When the shear span ratio is larger, SRCH columns are destroyed in the flexural failure mode because of the better ductility. However, when the shear span ratio is less, the ductility of the SRHC columns is so bad that these columns should be avoided in seismic design. The relationship of ductility factor with shear span ratio increase is shown in Fig. 13(a); As the axial load ratio increases, the ductility factor of the SRHC columns decreases as shown in Fig. 13(b). The larger axial load ratio leads to the principal compressive stress and strain of concrete rising because of the *P-Δ* effect, after which, the ability of deformation at the later stage of loading is abated. As the concrete strength increases, the ductility factor of the SRHC columns decreases as expected. The effect of concrete strength on the ductility of the specimens is mainly determined by the HPHC concrete characteristics. As the strength of the concrete increases, its ultimate

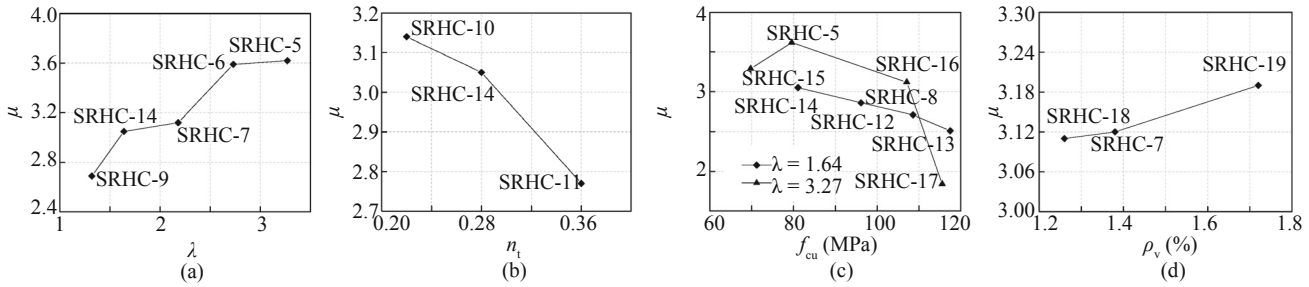

Fig. 13 The relationship between ductility factors and design parameters

strain decreases and brittleness become more obvious. Specimen ductility also lessens as shown in Fig. 13(c). As the stirrup ratio increases, the ductility factor of the specimens increases as shown in Fig. 13(d). The larger stirrups ratio can provide a good constraint to concrete due to the multidirectional compression which limits the development of the deformation. However, the ductility factor cannot always increase with the stirrup ratio increase. Therefore, it is not effective to only depend on increasing the stirrup ratio to improve the ductility of the SRHC frame columns.

3.5 Shear bearing capacity

When the structure is subjected to earthquake loading, the columns with large axial load ratio and less shear span ratio will be suddenly destroyed if the shearing capacity is not sufficient. Therefore, the better bearing capacity of the diagonal section is crucial to ensure the seismic safety of the structure. Based on the test results, the various design parameters are taken into consideration for the shear bearing capacity of the SRHC frame columns. The relationships between shear bearing capacities and design parameters are shown in Fig. 14.

The shear span ratio is the most important factor affecting the shear bearing capacity of the SRHC columns. From Fig. 14(a), the conclusion can be easily drawn that as the shear span ratio increases, the bearing capacity of specimens decreases accordingly. When the shear span ratio λ is equal to 1.64, the ultimate bearing capacity reaches a maximum value. Furthermore, the curve becomes more and more pronounced even as the shear span ratio increases, but when $2.18 < \lambda \leq 2.73$, the curve is more steep than that of $2.73 < \lambda \leq 3.27$. The impact of the shear span ratio on the bearing capacity of the specimens is mainly decided by their failure modes.

The occurrence of shearing failure in the SRHC frame columns is due to the stress in concrete reaching its ultimate strength. Therefore, concrete strength will have a significant influence on the shearing capacity

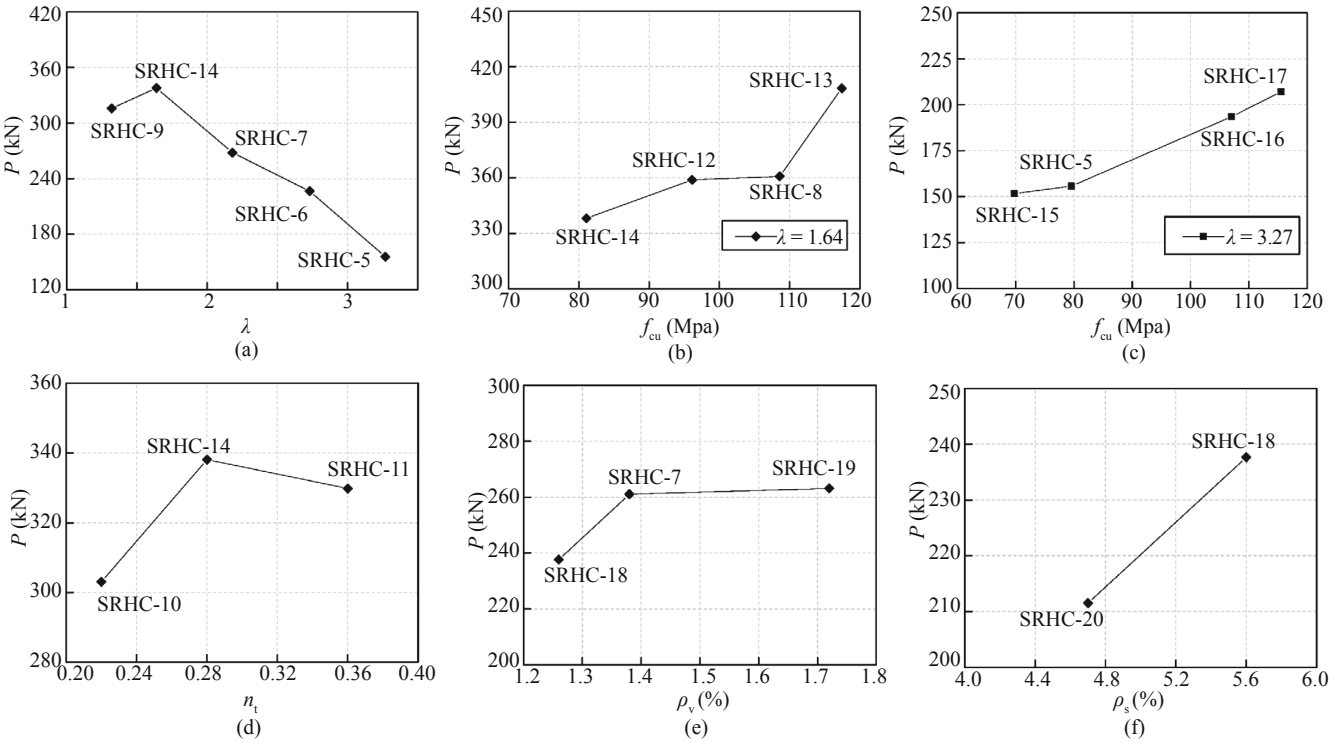

Fig. 14 The relationships between shear bearing capacity and design parameters

of the specimens (Figs. 14(b)–(c)). It can be easily concluded that if the other conditions are similar, the shearing capacity of the specimen will be greater when the concrete strength increases. However, the rate of increase for bearing capacity would be different when the shear span ratio is different. When the shear span ratio is small, the shearing capacity will increase sharply with an increase in concrete strength.

The axial compression ratio (as shown in Fig. 14(d)) also has an important effect on the bearing capacity of SRHC frame columns. First, the bearing capacity of the SRHC frame columns increases as the axial compression ratio increases. When the testing axial compression ratio is small ($n_t < 0.28$), shearing capacity increases rapidly corresponding to growth in the axial compression ratio. However, after that ratio increases to a certain degree ($n_t \geq 0.28$), the shearing capacity starts to gradually decrease. The effect of the axial compression ratio on the tested specimens must be within a certain domain (Jia *et al*., 2006; Li *et al*., 2007b).

The curve of shearing capacity versus stirrup ratio shows that the bearing capacity of the SRHC frame columns increases as the stirrup ratio increases. When the stirrup ratio is minor, the slope of the curve is large and the increasing speed of the shear capacity is sharp. This demonstrates that the effects of the stirrup ratio on the shearing capacity are relatively obvious. When the steel ratio increases, the shearing capacity of the specimens grows accordingly. Steel is the main bearing element and can effectively restrain interior concrete (Si *et al*., 2009; Jia, 2002). The relationship of the shearing capacity and stirrup ratio and steel ratio is illustrated in Figs. 14(e)–(f), respectively.

4 Calculation of shear capacity

4.1 Flexural failure mode

According to the experimental results, the failure modes of the specimens subjected to low-cycle repetitive loading can be divided into three types, namely flexural failure, shearing bond failure and shearing baroclinic failure. For flexural failure, strain distribution of steel and concrete satisfies the plane-section assumption in the preceding loading. However, because of the bond-slip effect in later loading, the plane-section assumption cannot be accurately met. Strain distribution presents a nonlinear property. The strain distribution of steel and concrete is shown in Figs. 15(a)–(b). To simplify the calculation, the modified plane-section assumption is adopted. This modified assumption means that the strain of the concrete and steel remains linear along the section when the column is in the ultimate state. The principle for establishing the modified plane-section assumption is to ensure that the height of the concrete compressive zone and the resultant force of the concrete compressive region are constant.

The failure mechanism of the flexural failure of the columns is similar to the compression failure with large eccentricity, as shown in Fig. 16. The ultimate strain of concrete for the modified plane-section assumption should consider the strong effect of concrete, which is defined as:

$$\varepsilon_{cu} = 0.0030 - \left(f_{cu,k} - 50\right) \times 10^{-5} \tag{1}$$

The characteristic coefficients of the concrete equivalent stress graph include α (ratio of corrected height, x of rectangle stress diagram, and height, x_0, of neutral axis) and β (ratio of corrected strength f_{cc} of rectangle stress diagram and maximum stress σ_0 of concrete in stress-strain relation). When $f_c < 50$ MPa, $\alpha = 0.8$, $\beta = 1.0$. When $f_c = 80$ MPa, $\alpha = 0.74$, $\beta = 0.94$. When $f_c = 120$ MPa, $\alpha = 0.69$, $\beta = 0.88$. The middle value is confirmed by the linear interpolation method. According to the modified plane-section assumption, the relationship can be taken as:

$$\frac{x_{b0}}{h - a_s} = \frac{x_{b0}}{h_0} = \frac{\varepsilon_c}{\varepsilon_c + \varepsilon_y} \tag{2}$$

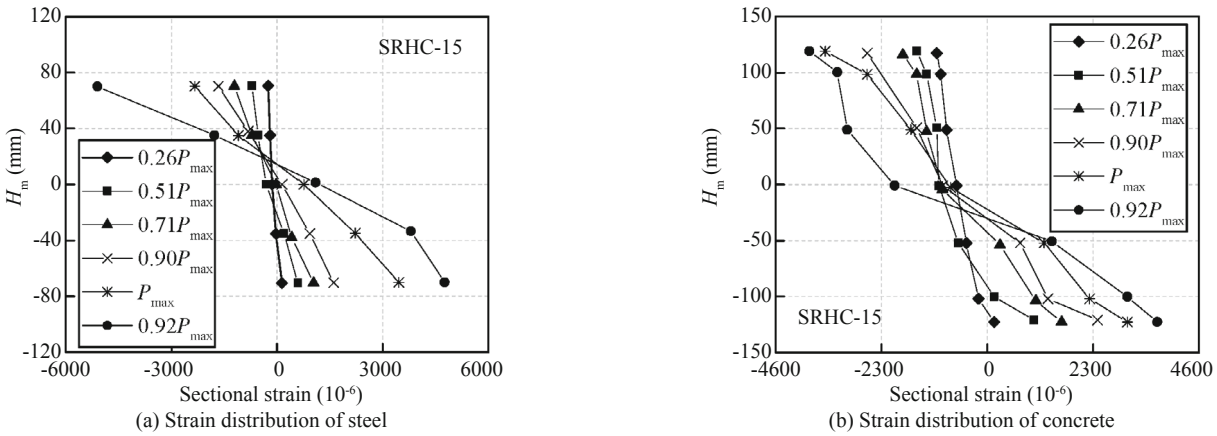

(a) Strain distribution of steel

(b) Strain distribution of concrete

Fig. 15 Strain distribution of steel and concrete for specimens with flexural failure mode

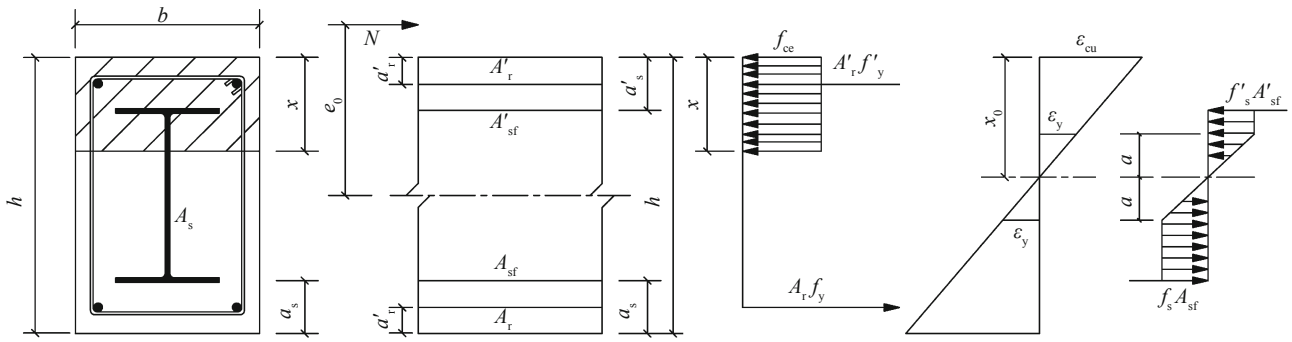

Fig. 16 Sectional stress and strain diagram of compression column with large eccentricity

$$\xi_b = \frac{x_b}{h_0} = \left(\frac{\alpha h_0}{1+\varepsilon_y/\varepsilon_c}\right)\Big/ h_0 = \frac{\alpha}{1+\varepsilon_y/\varepsilon_c} \tag{3}$$

When the columns collapse due to compression failure with large eccentricity, the tension flange of steel yield is the first problem followed by the concrete achieving ultimate compressive strain. According to force and moment equilibrium, it can be concluded that:

$$N_u = \beta f_c bx + f'_y A'_s + f'_s A'_{sf} + f'_s\left(\frac{1}{\alpha}x - a'_s - a\right)t_w - f_y A_s - f_s A_{sf} - f_s\left(h - a_s - \frac{1}{\alpha}x - a\right)t_w \tag{4}$$

$$M_u = \frac{1}{2}\beta f_c bx^2 + f'_y A'_s\left(\frac{1}{\alpha}x - a'_r\right) + f'_s A'_{sf}\left(\frac{1}{\alpha}x - a'_s\right) + f_y A_s\left(h - a_r - \frac{1}{\alpha}x\right) + f_s A_{sf}\left(h - a_s - \frac{1}{\alpha}x\right) + \frac{1}{2}f_s h_s^2 t_w - \frac{2}{3}f_s d^2 t_w \tag{5}$$

where (as shown in Fig. 16), b, h is the height and width of the cross section; h_s is the height of the I steel; t_w is the thickness of the I steel web plate; f_y' and f_y are the yield strength of the compression and tension reinforcement bars, respectively; A_r' and A_r are the area of pressed and pulled reinforcement, respectively; f_s' and f_s are the yield strength of compression and tension flange of the I steel, respectively; A_{sf}', A_{sf} is the area of pressed and pulled flange, respectively; a_s', a_r', a_s, and a_r are the distance from the edge of the section to the active point of the composite force of compression reinforcement, flange and tension reinforcement, and flange, respectively; a is the elastic height for the web plate of the I steel, and x is the height of the equivalent rectangular for concrete in the compressive zone; hence, $x = (N+f_s t_w h)/(\beta f_c b+2f_s t_w/\alpha)$.

Finally, the ultimate horizontal force P_u can be defined by

$$P_u = \frac{M_u}{H - \psi h} \tag{6}$$

where ψ is the effect coefficient for considering column bottom confinement, ψ = 0.2–0.5, and in this study, ψ is 0.38 approximately.

The calculation results of the bearing capacity are listed in Table 5. When the SRHC columns collapsed with flexural failure mode, the mean value of the ratio of the experimental value to calculation value was 1.081, and the variance was 0.041. The calculation values are in good agreement with the experimental values, which meet the design requirements of bearing capacity for the SRHC frame.

4.2 Shear bond failure mode

When the shearing bond failure occurs, the bond effect of steel and concrete is basically lost. Thus

$$P_u = P_s + P_{hc} + P_{sv} \tag{7}$$

where P_u is the bearing capacity of the specimens; P_{hc} is the bearing capacity of the high strength and high performance concrete; P_s is bearing capacity of the I

Table 5 Comparison of experimental values and calculation values for bearing capacity of SRHC frame columns

Specimen	f_{cu} (MPa)	λ	n_t	ρ_v (%)	ρ_s (%)	P_m (kN)	P_c (kN)	P_m/P_c
SRHC-5	79.58	3.27	0.28	1.38	5.60	155.72	143.79	1.083
SRHC-6	85.49	2.73	0.31	1.38	5.60	226.60	200.89	1.128
SRHC-15	69.75	3.27	0.26	1.38	5.60	151.59	142.87	1.061
SRHC-16	107.07	3.27	0.27	1.38	5.60	193.51	172.93	1.119
SRHC-17	115.52	3.27	0.31	1.38	5.60	206.97	204.11	1.014
Average		1.081		Standard deviation		0.041		

steel; P_{sv} is the bearing capacity of the stirrups.

4.2.1 Bearing capacity of I steel

Considering a simplified calculation, the assumption is: steel is all plasticity; steel web resists all shear force; steel web and flange resist moment and axial force together; the direct stress and shear stress in the steel web are all uniform distribution and satisfy Mises yield condition, namely

$$\left(\frac{\sigma}{f_s}\right)^2+3\left(\frac{\tau}{f_s}\right)^2=1 \tag{8}$$

where f_s is the yield stress of steel; and σ and τ are the direct stress and shear stress of the steel section, respectively. According to the equilibrium condition of force and boundary condition, the following equations can be given.

$$P_s=t_w h_w \tau \tag{9}$$

$$M_s=b_f h_f\left(t_w+h_f\right)f_s+\frac{1}{4}t_w h_w^2\sigma \tag{10}$$

$$M_s=P_s h_l \tag{11}$$

The following monadic quadratic equation can be presented by the upper simultaneous equations.

$$\begin{aligned}&\left(16h_l^2+3h_w^2\right)P_s^2-32Hb_f h_f\left(t_w+h_f\right)f_s P_s+\\&\left[16b_f^2h_f^2\left(t_w+h_f\right)^2-t_w^2h_w^4\right]f_s^2=0\end{aligned} \tag{12}$$

Finally, the solution is

$$P_s=\frac{4h_l B+\sqrt{\left(16h_l^2-A\right)B^2+3AC}}{A}f_s \tag{13}$$

where $A = 16H^2+3\,h_w^2$; $B = 4b_f h_f(h_w+h_f)$; $C = t_w^2\ h_w^4$. P_s and M_s are the bearing capacity and bending moment of the I steel, respectively; h_l is the height of the I steel; b_f and h_f are the width and thickness of the I steel flange, respectively; and h_w and t_w are the height and thickness of the I steel web plate, respectively.

4.2.2 Bearing capacity of high strength and high performance concrete

The force diagram of the specimen for bond failure is shown in Fig. 17. N_1 and N_2 are the resultant of axial force, whose application point is in the gravity center. The transverse compression stress σ in the splitting plane generates from the stirrup constraint effect, which is considered as a uniform distribution, then

$$\sigma=\frac{A_{sv}}{bs}\sigma_{yv}=\rho_{sv}\sigma_{yv} \tag{14}$$

where A_{sv} is the sum of the stirrup area in the identical section; b is the width of the specimens; s is the space length of the stirrups; and σ_{yv} is the stress of the stirrups. The test results indicate that when the load reaches maximum, the strain of a stirrup is about 0.4–0.6 of the yield strain. Sampling $\sigma_{yv} = 0.5f_{yv}$, namely

$$\sigma=0.5\rho_{sv}f_{yv} \tag{15}$$

The shearing stress τ in the splitting plane includes two parts: bond stress τ_1 of steel and concrete and concrete shearing stress τ_2 in two sides of steel flange, then

$$\tau_1=\lambda_{cy}\left(0.2378+0.4480\,C_{ss}/h_s\right)f_t \tag{16}$$

where C_{ss} is the thickness of the covering layer; h_s is the height of the I steel; f_t is the tensile strength of the concrete; λ_{cy} is the degeneration factor for bond stress of the specimen subjected to repetitive loading, and λ_{cy} = 0.83. The principal tensile stress of the concrete element in the splitting plane is described as

$$\sigma_1=-\frac{\sigma}{2}+\frac{1}{2}\sqrt{\sigma^2+4\tau_1^2} \tag{17}$$

When $\sigma_1 = f_t$, splitting failure occurs. τ_1 can then be solved as:

$$\tau_1=\sqrt{f_t\left(f_t+0.5\rho_{sv}f_{yv}\right)} \tag{18}$$

According to the boundary condition (shown in Fig. 17), the following equation can be given:

$$a\mathrm{d}N_1=\mathrm{d}M_{rhc} \tag{19}$$

$$\frac{\mathrm{d}N_1}{\mathrm{d}x}d=\frac{\mathrm{d}M_{hc}}{\mathrm{d}x}=P_{hc} \tag{20}$$

$$\mathrm{d}N_1=\left[\tau_1\left(b-b_f\right)+\tau_2 b_f\right]\mathrm{d}x \tag{21}$$

P_{hc} is given by the following equation:

$$P_{hc}=\left[\tau_1\left(b-b_f\right)+\tau_2 b_f\right]d \tag{22}$$

where d is the arm of the inner force, $d = 0.875\ h$. Finally, introducing the value of τ_1, τ_2, the result is

$$\begin{aligned}P_{hc}=0.875h\Big[&\sqrt{f_t\left(f_t+0.5\rho_{sv}f_{yv}\right)}\left(b-b_f\right)+\\&0.830\times\left(0.2378+0.4480\,C_{ss}/h_s\right)f_t b_f\Big]\end{aligned} \tag{23}$$

4.2.3 Bearing capacity of stirrups

The shear bearing capacity P_{sv} of stirrup is presented by

$$P_{sv}=1.25\sigma_{yv}\frac{A_{sv}}{s}h_0 \tag{24}$$

where h_0 is the sectional effective height, $h_0 = h-a_s$, a_s, which is the distance from the resultant point of tension reinforcement to the sectional tensile region edge.

The calculation results of the bearing capacity are listed in Table 6 when the SRHC columns collapse under the shear bond failure mode. The mean value of the ratio with experimental value to calculation value is 1.060, and the variance is 0.0392. The calculation values are

Table 6 Comparison of experimental values and calculation values for bearing capacity of SRHC frame columns

Specimen	f_{cu} (MPa)	λ	n_t	ρ_v (%)	ρ_s (%)	P_m (kN)	P_c (kN)	P_m/P_c
SRHC-7	79.38	2.18	0.28	1.38	5.60	261.06	249.82	1.045
SRHC-18	77.65	2.18	0.24	1.26	5.60	237.65	232.31	1.023
SRHC-19	80.69	2.18	0.23	1.72	5.60	263.12	251.55	1.046
SRHC-20	75.68	2.18	0.21	1.26	4.70	211.52	187.85	1.126
Average		1.060		Standard deviation		0.0392		

in good agreement with the experimental values, which meet the design requirements of the bearing capacity for the SRHC frame.

4.3 Shear baroclinic failure mode

The baroclinic failure mechanism is different from bond failure because the baroclinic strut of concrete is crushing. Thus

$$P_u = P_s + P_{rhc} \tag{25}$$

where P_u is the shear bearing capacity of the specimens; P_{rhc} is the shear bearing capacity of the reinforced high strength and high performance concrete; and P_s is the shear bearing capacity of the I steel which is calculated from previous section.

The force diagram of reinforced high strength and high performance concrete (RHC) for shearing compression failure is shown in Fig. 18, where C is the longitudinal resultant force of the concrete's baroclinic strut and compressive steel reinforcement; B is the resultant force of the concrete's baroclinic strut; α is the dip angle between the axis and the strut; and σ_r and A_r are the stress and area of pulled reinforcement, respectively. H is height of column.

The basic calculation assumption is that the load is assumed mostly by concrete baroclinic strut and steel reinforcements. When the compressive stress of the concrete baroclinic strut reaches f_c, the stress of the longitudinal reinforcements in the compressive region arrives at a yield strength of f_y synchronously. The shear bearing capacity P_{rhc} of the reinforced concrete includes two parts: 1) horizontal component force P_c of the concrete baroclinic strut and 2) resultant force P_{sv} of a stirrup, namely

$$P_{rhc} = P_c + P_{sv} \tag{26}$$

The analytical force diagram of RHC is shown in Fig. 18. It is divided into two parts (Gosain *et al*., 1977), the concrete baroclinic strut shearing element and stirrup shearing element. σ_{r1} and σ_{r2} are the stress of the tensile reinforcements in two parts, respectively; σ'_{r1} and σ'_{r2} are the stress of the compressive reinforcements in two parts, respectively. Then

$$\sigma_r = \sigma_{r1} + \sigma_{r2} \tag{27}$$

$$f_y = \sigma'_{r1} + \sigma'_{r2} \tag{28}$$

where f_y is the yield strength of the reinforcements; C_1 is the compressive composite force and satisfies the following equation:

$$C_1 = P\cos\alpha + \sigma'_{r1}A'_s \tag{29}$$

where A_s and A'_s are the sectional area of tensile and compressive reinforcements, respectively. w is the width of the concrete baroclinic strut and is calculated by

$$w = h - H\tan\alpha \tag{30}$$

4.3.1 Bearing capacity of stirrups

The stirrup is treated equivalently as a sheet along the column height. t is the thickness of the sheet, which is solved by the volume equivalent principle, namely

$$h_0 Ht = \frac{H}{s}A_{sv}h_0 \tag{31}$$

That is

$$t = \frac{A_{sv}}{s} \tag{32}$$

where h_0 is the length of the stirrup, approximately $h_0 = h\text{-}a_s$. Supposing the equivalent sheet resists shear force, longitudinal reinforcements take on moment and the foxtail effect is ignored, then

$$P_{sv} = \gamma h_0 t f_{yv} = \gamma\frac{A_{sv}}{s}h_0 f_{yv} = \gamma\rho_{sv}bh_0 f_{yv} \tag{33}$$

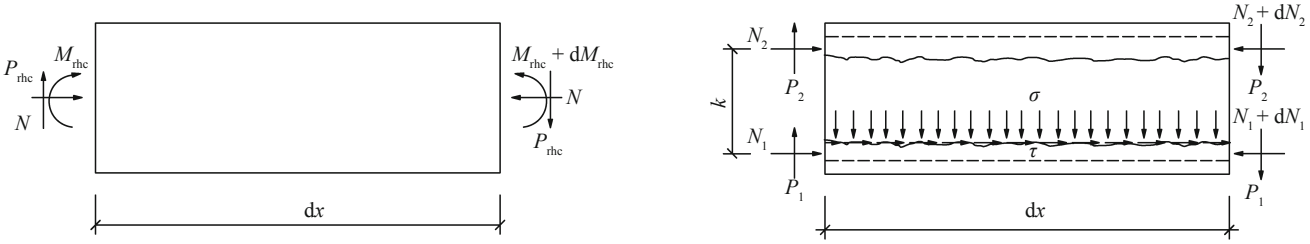

Fig. 17 Force diagram of specimen for bond failure

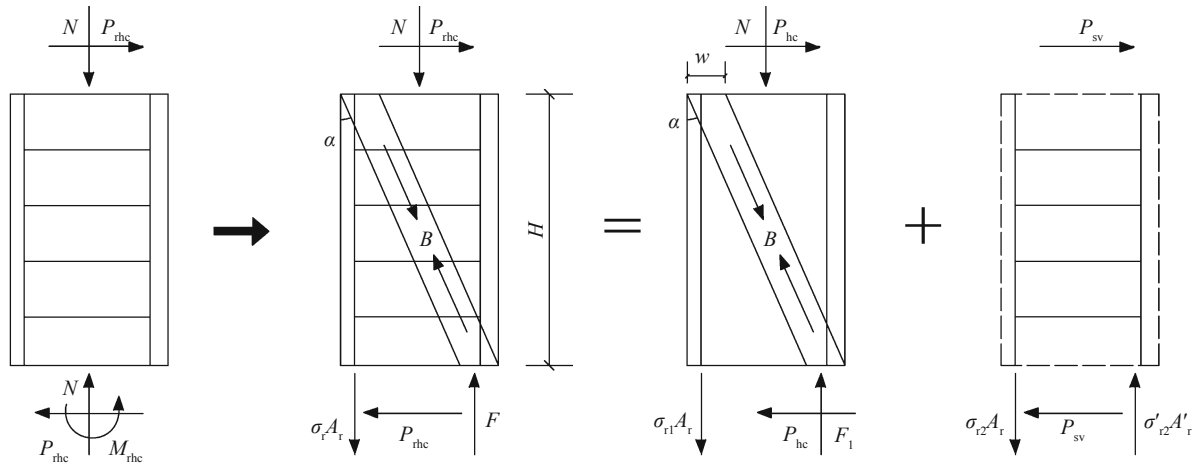

Fig. 18 Force diagram of RHC part for shearing compression failure

$$P_{sv}H = \sigma'_{r2}A'_s\left(h_0 - a_s\right) \tag{34}$$

where γ is the shearing coefficient of the stirrup, $\gamma = 0.6$; f_{yv} and ρ_{sv} are the yield strength of the stirrup and area stirrup ratio respectively; hence $\rho_{sv} = A_{sv}/(bs)$.

4.3.2 Bearing capacity of high strength and high performance concrete

According to the equilibrium condition of the concrete baroclinic strut shearing element, the following equations can be given:

$$P_c = B\sin\alpha = f_c bx\cos\alpha\sin\alpha = f_c b\left(h - H\tan\alpha\right)\cos\alpha\sin\alpha \tag{35}$$

$$N = C_1 - \sigma_{r1}A_s = B\cos\alpha + \sigma'_{r1}A'_s - \sigma_{r1}A_s \tag{36}$$

$$P_c H = \sigma_{r1}A_s d + N\left(d - h_0/2\right) \tag{37}$$

The derivation result is that

$$\sigma'_{r1}A'_s = N + \frac{P_c}{d}H - \frac{N}{d}\left(d - \frac{h_0}{2}\right) - B\cos\alpha \tag{38}$$

$$\sigma'_{r2}A'_s = \frac{H}{h_0 - a_s}P_{sv} \tag{39}$$

Based on Eq. (28), thus

$$N + \frac{P_c}{d}H - \frac{N}{d}\left(d - \frac{h_0}{2}\right) - B\cos\alpha + \frac{H}{h_0 - a_s}P_{sv} = f_y A'_s \tag{40}$$

Namely

$$f_c b\left(h - H\tan\alpha\right)d\cos^2\alpha - f_c bH\left(h - H\tan\alpha\right)\cdot \cos\alpha\sin\alpha + \left(f_y A'_s - \frac{H}{h_0 - a_s}P_{sv}\right)d - \frac{h_0}{2}N = 0 \tag{41}$$

Arranging as

$$\tan^2\alpha\left(\lambda H\frac{h}{h_0} - n_{rhc}\frac{h_0}{2} + d\rho_{cs}\frac{f_y}{f_c} - d\alpha\rho_{sv}\frac{H}{h_0 - a_s}\frac{f_{yv}}{f_c}\right) - \tan\alpha\left(d\lambda\frac{h}{h_0} + \frac{h}{h_0}H\right) + \left(d\frac{h}{h_0} - n_{rhc}\frac{h_0}{2} + d\rho_{cs}\frac{f_y}{f_c} - d\gamma\rho_{sv}\frac{H}{h_0 - a_s}\frac{f_{yv}}{f_c}\right) = 0 \tag{42}$$

where λ is the shear span ratio, $\lambda = H/h$, and when $\lambda > 1.5$, $\lambda = 1.5$; n_{rhc} is the axial compression ratio of reinforced concrete, $n_{rhc} = N/(f_c bh_0)$, and when $n_{rhc} > 0.4$, $n_{rhc} = 0.4$; ρ_{cs} is the compressive reinforcement ratio, $\rho_{cs} = A'_s/(bh_0)$; d is the distance of the resultant force point of the tensile reinforcements to the resultant force point of the compressive zone. Valuing $d = 0.9h_0$ and $h = 1.1\ h_0$ approximately; hence, the following expression will be given:

$$\tan^2\alpha\left(1.1\lambda^2 - 0.45n_{rhc} + 0.81\rho_{cs}\frac{f_y}{f_c} - \lambda\alpha\rho_{sv}\frac{f_{yv}}{f_c}\right) - 2\lambda\tan\alpha + \left(0.9 - 0.45n_{rhc} + 0.81\rho_{cs}\frac{f_y}{f_c} - \lambda\gamma\rho_{sv}\frac{f_{yv}}{f_c}\right) = 0 \tag{43}$$

Assuming

$\kappa = -0.45n_{rhc} + 0.81\rho_{cs}\,f_y/f_c - \lambda\gamma\rho_{sv}\,f_{yv}/f_c$, then

$$\tan^2\alpha\left(1.1\lambda^2 + \kappa\right) - 2\lambda\tan\alpha + 0.9 + \kappa = 0 \tag{44}$$

Accordingly

$$\tan\alpha = \frac{2\lambda - \sqrt{4\lambda^2 - 4\left(1.1\lambda^2 + \kappa\right)\left(0.9 + \kappa\right)}}{2\left(1.1\lambda^2 + \kappa\right)} \tag{45}$$

Finally, P_c is given by following equation:

$$P_c = f_c bh\left(1 - \lambda\tan\alpha\right)\frac{\tan\alpha}{1 + \tan^2\alpha} \tag{46}$$

The calculation results of the bearing capacity are listed in Table 7. After the SRHC columns have collapsed under the shear baroclinic failure mode, the mean values of the ratio with experimental value to calculation value is 1.055, and the variance is 0.066. The calculation values are in good agreement with the experimental values, which meet the design requirements of bearing capacity for the SRHC frame.

5 Conclusions

Based on the low-cycle repetitive loading test and theoretical analysis of the SRHC frame columns, the following conclusions can be generalized:

(1) All seismic performance indexes of SRHC frame columns designed properly are adequate and can be applied in engineering practice. However, due to the natural brittleness of HSHPC, their ductility and energy dissipation capacity are inferior to those of ordinary SRC frame columns. Therefore, the axial compression ratio should be strictly limited, and some construction strengthening measures such as increasing stirrups should be adopted.

(2) As the shear span ratio increases, the failure modes of the specimens subjected to the compound action of compression, bending and shearing are ordinal shearing compression failure, shearing splitting failure and flexural failure, and the horizontal bearing capacity decreases gradually but the rate of deterioration slows down after the maximum horizontal load. The ductility and energy dissipation capacity is gradually enhanced.

(3) As the concrete strength and axial compression ratio heighten, the horizontal bearing capacity increases gradually but the rate of decay increases after the maximum horizontal load. The ductility and energy dissipation capacity reduce gradually.

(4) When the stirrup ratio and steel ratio grow, the horizontal bearing capacity increases gradually, and the rate of deterioration slows down. The ductility and energy dissipation capacity intensifies gradually.

(5) The calculation method proposed for shear bearing capacity of SRHC frame columns in different failure modes is reasonable and its corresponding expressions are accurate; hence, they can be applied to engineering design.

Acknowledgment

This study was funded by the National Key Technology R&D Program under Grant No. 2013BAJ08B00 and the Natural Science Foundation of China under Grant Nos. 50978218 and 51108376. The authors declare that they have no conflict of interest.

References

Abed F, Alhamaydeh M and Abdalla S (2013), "Experimental and Numerical Investigations of the Compressive Behavior of Concrete Filled Steel Tubes (CFSTs)," *Journal of Construction Steel Research*, **80**: 429−439.

Bae S and Bayrak O (2008), "Seismic Performance of Full Scale Reinforced Concrete Columns," *ACI Structural Journal*, **105**(2): 123–133.

Bayrak O and Sheikh SA (1997), "High-strength Concrete Columns under Simulated Earthquake Loading," *ACI Structural Journal*, **94**(6): 708–722.

Clough RW and Penzien J (2003), *Dynamics of Structures*, USA, Computers & Structures, Inc.

Gosain NK, Brown RH and Jirsa JO (1977), "Shear Requirements for Load Reversals on RC Members," *Journal of Structural Engineering*, **103**(7): 1461–1476.

JGJ138-2001 (2001), *Technical Specification for Steel Reinforced Concrete Composite Structure*, Beijing: China Building Industry Press. (in Chinese)

Ji Xiaodong, Sun Ya, Qian Jiaru, *et al*. (2015), "Seismic Behavior and Modeling of Steel Reinforced Concrete (SRC) Walls," *Earthquake Engineering and Structural Dynamics*, **44**(6): 955–972.

Jia Jinqing (2002), "Influence of Stirrup Ratio on Limiting Value of Ratio of Axial Compression Stress to Strength for Steel High-strength Concrete Columns," *China Civil Engineering Journal*, **35**(6): 39–43. (in Chinese)

Jia Jinqing, Jiang Rui and Hou Tong (2006), "An Experimental Study on the Seismic Performance of Steel Reinforced Super High-strength Concrete Columns," *China Civil Engineering Journal*, **39**(8): 14–18. (in Chinese)

Table 7 Comparison of experimental values and calculation values for shear bearing capacity of SRHC frame columns

Specimen	f_{cu} (MPa)	λ	n_t	ρ_v (%)	ρ_s (%)	P_m (kN)	P_c (kN)	P_m/P_c
SRHC-8	108.56	1.64	0.32	1.38	5.60	360.72	318.66	1.132
SRHC-9	78.49	1.32	0.22	1.38	5.60	315.85	336.73	0.938
SRHC-10	80.19	1.64	0.22	1.38	5.60	302.95	274.41	1.104
SRHC-11	79.42	1.64	0.36	1.38	5.60	329.79	318.64	1.035
SRHC-12	96.14	1.64	0.26	1.38	5.60	358.89	324.49	1.106
SRHC-13	117.42	1.64	0.31	1.38	5.60	408.45	376.45	1.085
SRHC-14	81.07	1.64	0.28	1.38	5.60	338.04	342.49	0.987
Average		1.055		Standard deviation		0.066		

Kamal MM, Safan MA, Etman ZA, *et al*. (2014), "Behavior and Strength of Beams Cast with Ultra High Strength Concrete Containing Different Types of Fibers," *HBRC Journal*, **10**(1): 55–63.

Li Junhua, Wang Xintang, Xue Jianyang, *et al*. (2007a), "Experimental Study on the Performance of Steel Reinforced High-strength Concrete Columns under Low Cyclic Reversed Loading," *China Civil Engineering Journal*, **40**(7): 11–18.(in Chinese)

Li Junhua, Wang Xintang, Xue Jianyang, *et al*. (2007b), "Experimental Study on the Limit Values of Axial Compressive Ratio of Steel Section High-strength Concrete Columns," *World Earthquake Engineering*, **23**(2): 154–160. (in Chinese)

Lu Yanlu, Li Na, Li Shan, *et al*. (2015), "Experimental Investigation of Axially Loaded Steel Fiber Reinforced High Strength Concrete-filled Steel Tube Columns," *Journal of Central South University*, **22**(6): 2287–2296.

Ricles JM, Member A and Paboojian SD (1994), "Seismic Performance of Steel-encased Composite Columns," *Journal of Structural Engineering*, **120**(8): 2474–2494.

Si Bingjun, Sun Zhiguo, Wang Dongsheng, *et al*. (2009), "Review of Studies on the Seismic Behavior of High Strength Concrete Columns with High Strength Transverse Reinforcement," *China Civil Engineering Journal*, **42**(4): 1–9. (in Chinese)

Wang Lianguang (2005), *Theory and Calculation of Steel and Concrete Composite Structure*, Beijing: Science Press. (in Chinese)

Xia Jun, Mackie KR, Saleem MA, *et al*. (2011), "Shear Failure Analysis on Ultra-high Performance Concrete Beams Reinforced with High Strength Steel," *Engineering Structures*, **33**(12): 3597–3609.

Yan Changwang and Jia Jinqing (2010), "Seismic Performance of Steel Reinforced Ultra High-strength Concrete Composite Frame Joints," *Earthquake Engineering and Engineering Vibration*, **9**(3): 439–448.

Zheng Shansuo, Wang Bin, Li Lei, *et al*. (2011), "Study on Seismic Damage of SRHSC Frame Columns," *Science China Technological Sciences*, **54**(11): 2886–2895.